

Assessing the reliability of peatland GPP measurements by remote sensing: from plot to landscape scale

Article

Accepted Version

Creative Commons: Attribution-Noncommercial-No Derivative Works 4.0

Lees, K. J., Khomik, M., Quaife, T. ORCID:
<https://orcid.org/0000-0001-6896-4613>, Clark, J. M. ORCID:
<https://orcid.org/0000-0002-0412-8824>, Hill, T., Klein, D.,
Ritson, J. and Artz, R. R. E. (2021) Assessing the reliability of
peatland GPP measurements by remote sensing: from plot to
landscape scale. *Science of the Total Environment*, 766.
142613. ISSN 0048-9697 doi:
<https://doi.org/10.1016/j.scitotenv.2020.142613> Available at
<https://centaur.reading.ac.uk/93388/>

It is advisable to refer to the publisher's version if you intend to cite from the work. See [Guidance on citing](#).

To link to this article DOI: <http://dx.doi.org/10.1016/j.scitotenv.2020.142613>

Publisher: Elsevier

All outputs in CentAUR are protected by Intellectual Property Rights law, including copyright law. Copyright and IPR is retained by the creators or other copyright holders. Terms and conditions for use of this material are defined in the [End User Agreement](#).

www.reading.ac.uk/centaur

CentAUR

Central Archive at the University of Reading

Reading's research outputs online

1 Assessing the reliability of peatland GPP measurements by 2 remote sensing: from plot to landscape scale.

3 **Kirsten J Lees^{1,2*}, Myroslava Khomik³, Tristan Quaife⁴, Joanna M Clark¹, Tim Hill²,
4 Daniela Klein⁵, Jonathan Ritson⁶, and Rebekka RE Artz⁷**

- 5
6 1. Department of Geography and Environmental Science, University of Reading, Whiteknights, RG6 6DW,
7 UK.
8 2. Department of Geography, University of Exeter, Streatham Campus, Exeter, EX4 4QE, UK
9 3. University of Waterloo, ON N2L 3G1, Canada
10 4. National Centre for Earth Observation, Department of Meteorology, University of Reading, Reading,
11 Whiteknights, RG6 6BB, UK.
12 5. Forsinard Flows RSPB Office, Forsinard, KW13 6YT, UK
13 6. Imperial College London, SW7 2A7 UK
14 7. The James Hutton Institute, Craigiebuckler, Aberdeen, AB15 8QH, UK

15 **Abstract.** Estimates of peatland carbon fluxes based on remote sensing data are a useful addition to monitoring
16 methods in these remote and precious ecosystems, but there are questions as to whether large-scale estimates are
17 reliable given the small-scale heterogeneity of many peatlands. Our objective was to consider the reliability of
18 models based on Earth Observations for estimating ecosystem photosynthesis at different scales using the
19 Forsinard Flows RSPB reserve in Northern Scotland as our study site. Three sites across the reserve were
20 monitored during the growing season of 2017. One site is near-natural blanket bog, and the other two are at
21 different stages of the restoration process after removal of commercial conifer forestry. At each site we measured
22 small (flux chamber) and landscape scale (eddy covariance) CO₂ fluxes, small scale spectral data using a handheld
23 spectrometer, and obtained corresponding satellite data from MODIS. The variables influencing GPP at small
24 scale, including microforms and dominant vegetation species, were assessed using exploratory factor analysis. A
25 GPP model using land surface temperature and a measure of greenness from remote sensing data was tested and
26 compared to chamber and eddy covariance CO₂ fluxes; this model returned good results at all scales (Pearson's
27 correlations of 0.57 to 0.71 at small scale, 0.76 to 0.86 at large scale). We found that the effect of microtopography
28 on GPP fluxes at the study sites was spatially and temporally inconsistent, although connected to water content
29 and vegetation species. The GPP fluxes measured using EC were larger than those using chambers at all sites, and
30 the reliability of the TG model at different scales was dependent on the measurement methods used for calibration
31 and validation. This suggests that GPP measurements from remote sensing are robust at all scales, but that the
32 methods used for calibration and validation will impact accuracy.

33
34 **Keywords:** TG model, photosynthesis, NDVI, satellite, blanket bog

35
36 *Corresponding author: K.lees@exeter.ac.uk
37

38 1 Introduction

39 Peatlands are important ecosystems for carbon sequestration, but many areas in the Northern
40 Hemisphere have experienced degradation through human land use. As an organic-rich, water-
41 saturated substrate, peat stores huge amounts of carbon relative to the land area it occupies due
42 to inhibited decomposition. In Scotland, peatlands store 56% of total soil carbon whilst
43 occupying 24% of the land area (Chapman *et al.*, 2009). Many peatland areas have, however,
44 been subject to managements such as draining, grazing, burning and planting for commercial

45 forestry, which have reduced saturation and increased bulk density of the peat (JNCC, 2011).
46 Restoration of peatland areas is of interest to policy makers as a carbon emissions abatement
47 scheme (IUCN, 2016; European Commission, 2018), but needs to be based on a robust
48 understanding of peatland ecosystems in order to effectively reverse previous damage.
49 Practitioners need techniques to assess changes in peatland carbon fluxes at a landscape scale
50 in order to measure the success of restoration processes and detect where to focus further
51 efforts.

52 Upscaling of ecosystem processes is an important research area in ecology, as landscape and
53 regional scale estimates are needed for policy decisions and carbon accounting (Fu *et al.*, 2014;
54 Le Clec'h *et al.*, 2018). Blanket bogs (peatland covering large areas and sustained by rainfall
55 and relatively low annual temperature fluctuations (Lindsay, 2010)) in particular have small-
56 scale heterogeneity in topographic features known as hummocks and hollows, which can vary
57 at scales of less than a metre (Belyea and Clymo, 2001). This microtopographical variation
58 influences vegetation communities, which can induce significant variation in carbon fluxes
59 (Dinsmore *et al.*, 2009; Arroyo-Mora *et al.*, 2018; Peichl *et al.*, 2018).

60 Conventional methods of carbon dioxide (CO₂) exchange measurement include flux chambers
61 and Eddy Covariance (EC) towers, both of which cover relatively small areas and are expensive
62 to manage and maintain. Remote sensing has the potential to help monitor carbon fluxes in
63 these important, remote and extensive areas that are difficult to access for conventional field-
64 based measurements as well as sensitive to trampling, yet little testing of methods has been
65 carried out (Lees *et al.*, 2018). The existence of satellites with very fine spatial resolution (to
66 tens of metres in freely accessible data) means that studies can now consider variation within
67 a landscape, but the microtopography of blanket bogs is still at a scale that is too fine to be
68 detectable from non-commercial satellite data (Becker *et al.*, 2008). Models using satellite data
69 to estimate carbon fluxes are being developed to cover large areas (Lees *et al.*, 2018) and have

70 recently shown successes in estimating carbon fluxes from peatland landscapes (Kross,
71 Seaquist and Roulet, 2016; Lees, Quaife, *et al.*, 2019), but there is still uncertainty over whether
72 these models can adequately detect the variation from small-scale peatland heterogeneity
73 (Zhang *et al.*, 2007; Arroyo-Mora *et al.*, 2018). The focus of this study is therefore to assess
74 whether the small-scale variations in carbon fluxes due to microtopography can be detected
75 using remote sensing data, and whether large scale estimates using these techniques are a
76 reliable estimate of the average fluxes resulting from these mosaic landscapes.

77 A Temperature and Greenness (TG) model is specifically considered in this study, as this has
78 previously been shown to give good agreement with EC data over the same study area as used
79 in this work (Lees, Quaife, *et al.*, 2019). This model combines a measure of land surface
80 temperature with a vegetation index, in this case the Normalised Difference Vegetation Index
81 (NDVI), to give an estimate of Gross Primary Productivity (GPP).

82 The aim of this work is to consider what factors affect GPP in blanket bog, and whether the
83 results from large scale models using satellite data can give reliable estimates of photosynthesis
84 measurements made at smaller scales. We hypothesise that the TG model will give good
85 agreement with chamber flux data at the small scale, and with EC data at the larger scale. We
86 also expect that the measurements and estimates at different spatial scales will show similar
87 results in both patterns and values. The approaches are tested at the Forsinard Flows RSPB
88 (Royal Society for the Protection of Birds) reserve, which is an ideal study location as it has a
89 chronosequence of areas undergoing restoration from commercial forestry (Hancock *et al.*,
90 2018), and long-term Eddy Covariance (EC) monitoring of greenhouse gas emissions
91 (Hambley *et al.*, 2019) at several of the restoration sites.

92 **2 Methods**

93 *2.1. Field sites*

94 This research is based at three field sites within the Forsinard Flows RSPB reserve in Northern
95 Scotland (approx. 58.36, -4.04 to 58.43, -3.63, WGS84). The reserve is part of the much larger
96 blanket bog Flow Country EU Natura site. Cross Lochs is a near natural site (see Levy and
97 Gray, (2015), where no drainage has been applied. An EC tower is located at 58.3703,-3.9644
98 (WGS84), elevation 211 m.

99 Talaheel and Lonielist are both sites undergoing restoration, which were previously drained
100 and subsequently planted for commercial conifer (sitka spruce *Picea sitchensis* and lodgepole
101 pine *Pinus contorta*) forestry in the mid to late 1980s.

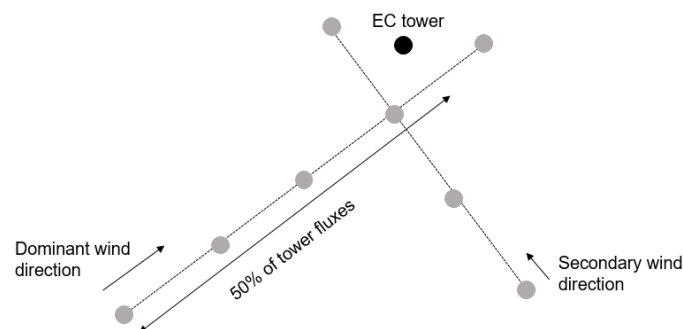
102 Talaheel was initially felled in 1998, with the trees laid into the planting furrows; some areas
103 have since undergone partial further landscaping (which affects half the points in this study) to
104 crush the decomposing conifer brash and to create peat dams in the furrows (winter 2015/16).
105 This has led to raised water levels across the site (see Hancock et al., 2018). The EC tower is
106 located at 58.4146, -3.8006 (WGS84), elevation 196 m.

107 The conifer plantation at Lonielist was felled in winter 2003/2004. At the time of measurement,
108 it retained the distinctive pattern of ridges on which the trees were planted, and drainage ditches
109 infilled with the felled trees. This site had undergone no further management until the end of
110 this project (-end of 2017). The EC tower is located at 58.3910, -3.7651 (WGS84), elevation
111 180 m.

112 All three sites are subject to some light grazing by wild red deer (*Cervus elephantis*). Talaheel
113 is fenced as part of a larger enclosure including some forestry, although some deer are present
114 inside the fence, whilst Lonielist and Cross Lochs are entirely open to grazing.

115 Small scale measurement points were set up in the area within each site's EC tower footprint.
116 The precise distances from the tower and dominant wind directions (Northwest and Southwest)
117 were determined from Hambley (2016) to incorporate appropriate locations within the average

118 flux tower footprints. At each site two perpendicular crossing transects were set up, one
 119 including five points and extending away from the tower into the dominant wind direction, and
 120 one including four points and extending into the secondary wind direction (see Figure 1). At
 121 Lonielist the main transect was 80 m and the secondary transect was 60 m, with all points 20
 122 m apart. At Talaheel the transects were 100 m and 75 m with the points 25 m apart, and at
 123 Cross Lochs the transects were 120 m and 90 m with points 30 m apart. At each point two PVC
 124 collars (24 cm in diameter) were placed: one on higher microforms (ridges in the restored sites,
 125 hummocks at Cross Lochs) and one on lower microforms (in the furrows at the restored sites,
 126 hollows at Cross Lochs); therefore, there were 16 collars at each of the three sites. The collars
 127 were 8 cm depth and were inserted to approximately 4 cm below ground. At least 24 hours
 128 were allowed between collar insertion and first measurements.



129

130 **Figure 1** – Location of points within the tower footprint. Two collars, one on a higher microform and one in a
 131 lower area, were placed at each point.

132

133 2.2. Chamber flux measurements

134 Monthly in situ CO₂ flux measurements beginning March and ending September 2017 were
 135 taken using a LICOR-8100A (LICOR Inc., Lincoln, Nebraska, USA) portable infrared gas
 136 analyser and custom Perspex chambers of 24 cm diameter and 30 cm height. Small 9V battery-
 137 operated fans were installed within the chambers to circulate the air. The two chambers, one
 138 clear and one covered with a blackout cloth, were sealed to the collars using rubber mastic

139 (Terostat), and consecutive measurements were taken with a brief aeration period as the
140 chambers were exchanged. Each measurement period was five minutes, with a 20 second pre-
141 measurement stabilisation period. Chamber flux measurements were usually taken between 8
142 am and 2 pm, although this was sometimes altered due to weather conditions. Each collar was
143 measured once with a clear-chamber and once with a blackout chamber on each visit except
144 when adverse weather conditions prevented a full dataset being collected.

145 *2.3. Field spectrometry*

146 Spectral measurements in the field were taken on the same visits as the chamber flux data
147 collection using a handheld SVC HR-1024 (Spectra Vista Corporation, spectral resolution 3.5
148 to 9.5 nm) spectroradiometer mounted on a monopod and held approximately 1m from the
149 surface using an 8° FOV lens with an on-the-ground footprint within the diameter of the collars.
150 The spectral range of the instrument is from 337 nm to 2521 nm. Three measurements were
151 taken of the vegetation within each collar, at three different angles to minimise structural effects
152 (opposite the position of the sun and at 90° to either side). A Spectralon reference panel was
153 also measured before each observation (within a minute) to normalise from radiance to
154 reflectance.

155 The Normalised Difference Vegetation Index (NDVI) is calculated from the difference
156 between reflectance in red wavelengths of light, which plants absorb strongly, and the near-
157 infrared (NIR), which plants reflect:

$$158 \text{NDVI} = (R_{\text{NIR}} - R_{\text{red}}) / (R_{\text{NIR}} + R_{\text{red}}) \quad (1)$$

159 In this study we calculated the red and NIR bands as the average of the values in wavelengths
160 630-680 nm and 845-885 nm respectively.

161 *2.4. Other factors measured in the field*

162 Photosynthetically Active Radiation (PAR) was measured outside the chamber during clear
 163 chamber measurements. Soil moisture was measured using a moisture probe with 6 cm prongs
 164 (Theta probe ML2x connected to HH2 moisture meter, Delta-T Devices). At the Lonielist site,
 165 dipwells were inserted within a metre of each collar, and the water level was monitored
 166 manually at the same time as the spectral measurements were taken. A lollipop thermometer
 167 (Fisherbrand, accurate to $\pm 1^\circ\text{C}$) was used to measure soil temperature outside the collar at two
 168 different depths, 5 cm and 15 cm. The thermometer was also used to measure temperature
 169 within the vegetation inside the chamber at the start and end of each flux measurement. These
 170 measurements were taken on the same dates and at the same plots as other monitoring (above).
 171 To consider the different vegetation communities of the microforms, the species within the
 172 collars were surveyed in June 2017. All species were recorded as percentage cover over the
 173 area of the collar, and overlapping canopies sometimes allowed total percentage cover to be
 174 over 100%. Six species which were found at all three sites were selected as indicators of
 175 microform vegetation communities. These are shown in Table I.

176 **Table I** – species selected which were present at all three sites, which microform they prefer, and their average
 177 (and standard deviation) percentage coverage in collars at each site.

178

Common name	Latin name	Hummock or Hollow	Lonielist	Talaheel	Cross Lochs
Heather	<i>Calluna vulgaris</i>	Hummock	7.5 \pm 11.7 %	4.7 \pm 9.8 %	9.7 \pm 9.5 %
Common cotton grass	<i>Eriophorum angustifolium</i>	Hollow	10.9 \pm 13.6 %	17.9 \pm 15 %	9.4 \pm 10.5 %
Reindeer lichen	<i>Cladonia portentosa</i>	Hummock	12.8 \pm 18 %	17.6 \pm 26.9 %	11.4 \pm 18.2 %
Red bogmoss	<i>Sphagnum capillifolium</i>	Hummock	19.9 \pm 22.5 %	16.7 \pm 30.1 %	27.7 \pm 18.1 %
Red-stemmed feather moss	<i>Pleurozium schreberi</i>	Hollow	12.3 \pm 22.1 %	23.6 \pm 27.9 %	3.9 \pm 7.2 %

Deer grass	<i>Trichiophorum germanicum</i>	Hollow	0.6 ± 2.5 %	4.9 ± 8.3 %	21.8 ± 21.6 %
------------	---------------------------------	--------	-------------	-------------	---------------

179

180 *2.5. Eddy Covariance*

181 Eddy covariance data from the whole of 2017 was used, except for Lonielist where data
182 collection began on the 24th of March.

183 Net ecosystem exchange of CO₂ (NEE) at Lonielist was measured using a LI-7200 enclosed
184 CO₂/H₂O infrared gas analyser (LI-COR Biosciences Inc. Lincoln, NE, USA), and a Gill HS-
185 50 3-D sonic anemometer (Gill Instruments, Lymington, UK). Data was collected at 20Hz
186 frequency and recorded every half-hour onto a 16GB USB by the LI-7550 Analyzer Interface
187 Unit (LICOR Biosciences, Inc. NE, USA). An insulated 1-meter intake tube was used and the
188 flow was controlled by the Flow Module (7200-101, Li-Cor Inc., Nebraska, USA) to be about
189 15L/min. The instruments were mounted on top of a scaffolding-tower at 2.90 m height,
190 pointing into the predominant wind direction (W-SW, 240° North offset).

191 At Talaheel, NEE was measured using the LI-7500A open path CO₂/H₂O gas analyser (LI-
192 COR Biosciences Inc. Lincoln, NE, USA) with a custom enclosure added to the analyser to
193 create an enclosed system (Clement *et al.*, 2009), and a CSAT sonic anemometer (Campbell
194 Scientific, Logan, USA) (Hambley *et al.*, 2019). Data was measured at 10Hz frequency and
195 recorded every half-hour on a flash-card by the CR5000 datalogger. Instruments were set-up
196 at 4.3 m height on a scaffolding tower.

197 At Cross Lochs NEE was measured by the IRGASON - an open-path infra-red gas analyser
198 integrated into a 3D-CSAT anemometer, and controlled by the EC100 electronics control
199 module (Campbell Scientific Ltd. UK). Data was measured at 10Hz, processed by the onboard
200 EasyFluxDL software (Campbell Scientific Ltd. UK) into half-hourly corrected and averaged
201 fluxes and recorded on a flashcard by the CR3000 datalogger. EasyFluxDL software processes

202 the EC data using commonly used corrections in the scientific literature (Campbell Scientific,
203 2016). The instruments were set up at 2.3 m height on a tri-pod tower, pointing 310° NW in
204 the predominant wind direction.

205 The flux data collected by the EC systems at Lonielist and Talaheel were processed using the
206 EddyPro® software (v7.0.4, Li-Cor Inc, Nebraska, USA), in Express mode, on a PC in the
207 office. Similar to EasyFluxDL, EddyPro® uses the most accepted and cited techniques in
208 scientific literature to compute fully-processed half-hourly fluxes. For more details on
209 EddyPro®, please see the EddyPro® manual (LI-COR Biosciences, 2017) and Fratini and
210 Mauder (2014). The processed half-hourly NEE fluxes from all three sites were further
211 processed in a custom R-software script (R Core Team, 2018) to quality check the data –
212 making sure that each half hour had at least 80% of records, that each half hour NEE value was
213 within 3.5 standard deviations of the running 10-hour means and that the data was within
214 physically plausible values for each ecosystem. Using R-code adapted from
215 "<http://footprint.kljun.net/download.php>" [November 2018]), a flux footprint analysis was
216 performed following Kljun *et al.* (2015) to ensure that all fluxes originated from within 80%
217 of the area of interest. Footprint filtered NEE fluxes were gap-filled and partitioned into GPP
218 and Re, following the methods and code (REddyProc, R-script) of Wutzler *et al.* (2018). This
219 script also estimated the u-star threshold for the data, which was used to further filter out data
220 during times of low turbulence, before partitioning and gap-filling.

221 Measurements at Lonielist began in March, so 23% of the data was missing at the start of the
222 2017 year. 26% of available (13550 hh) NEE half-hours were gap-filled at Lonielist, 52% at
223 Talaheel (of 17520 hh), and 60% at Cross Lochs (of 17520hh).

224 For comparison with the chamber and spectrometer data (TG1, see Section 2.7), the EC half-
225 hourly data covering the same time periods as the chamber flux measurements were used,
226 doubled to give an hourly timestep. For comparison with the TG model using MODIS data

227 (TG2, see Section 2.7), the EC fluxes were averaged across 8-day periods and then multiplied
228 to give daily values, following Lees, Quaife, *et al.* (2019).

229 2.6. Satellite data

230 The Moderate Resolution Imaging Spectroradiometer (MODIS) on satellite Terra was used in
231 this study as an example of a medium resolution broad band satellite, which is widely used in
232 environmental studies. Pixels containing the EC towers were downloaded for this analysis.
233 Two MODIS products were used in this study, the 250 m MOD13Q1 NDVI product (Didan,
234 2015), and the 1 km MOD11A2 Daytime Land Surface Temperature (LST) product (Wan,
235 Hook and Hulley, 2015). The NDVI product is given in 16-day periods, whilst the LST product
236 is given in 8-day periods. The MODIS data products were downloaded using the MODIS
237 ORNL web service through Matlab code (Santhana Vannan *et al.*, 2009). Cloud filtering was
238 applied to remove pixels extensively affected by cloud cover, whilst letting through data which
239 was affected by clouds but still useable (Lees, Quaife, *et al.*, 2019). Each of the MODIS
240 products contains information about the quality of the data in each pixel, and this was used to
241 select which 8-day or 16-day pixels were useable. MOD13Q1 pixel reliability index was used
242 to remove snow/ice or cloud affected values, whilst allowing marginal data. MOD11A2 quality
243 control data was used to remove periods when data was not produced due to cloud effects or
244 other issues. 17-50% of the data at each site were excluded following this protocol. Gap-filling
245 was then performed across each year using the techniques described by Wang *et al.* (2012),
246 before combining the data into the TG model.

247 2.7. The TG model

248 The Temperature and Greenness (TG) model combines a measure of temperature with a
249 vegetation index to give an estimate of GPP (Sims *et al.*, 2008). The model is formulated

250 following Moore et al. (2013), but using NDVI following the results of Lees, Quaife, *et al.*
 251 (2019):

$$252 \quad \text{GPP} = \text{NDVIs} \times \text{LSTs} \times m \quad (2)$$

$$253 \quad \text{NDVIs} = \text{NDVI} - 0.1 \quad (3)$$

$$254 \quad \text{LSTs} = \min[(\text{LST} - \text{minLST}) / (\text{optLST} - \text{minLST}), (\text{maxLST} - \text{LST}) / (\text{maxLST} - \text{optLST})] \quad (4)$$

255 Where NDVIs is the scaled Normalised Difference Vegetation Index and LSTs is the scaled
 256 Land Surface Temperature (see Sims *et al.*, 2008; Lees, Quaife, *et al.*, 2019). The scaled NDVI
 257 removes low values of NDVI which show no GPP. minLST, optLST and maxLST (given in
 258 °C) are the minimum, optimum and maximum Land Surface Temperature calculated for a
 259 specific ecosystem. We have used 40°C, 25°C and -2.5°C for maxLST, optLST and minLST
 260 respectively, following Lees, Quaife, *et al.*'s (2019) work on the same study sites. Furthermore,
 261 'm' is a site-optimisation parameter, and the GRG Nonlinear Solver in Microsoft Office Excel
 262 2013 was used to optimise this parameter at both small and large scales (see Section 4 for
 263 discussion of calibration).

264 Three different formulations of the TG model are used in this study to assess the effect of scale
 265 versus methodological bias. These versions are:

266 TG1 - Small-scale TG model using spectrometer data

267 The 'm' parameter for the TG model using spectrometer data was optimised to the chamber
 268 data across all months and sites and was given the value 0.4397. This small-scale version of
 269 the TG model gives an estimate of GPP per hour.

270 TG2 - Large-scale TG model using MODIS data

271 The ‘m’ parameter for the TG model using MODIS data was optimised to the EC data across
 272 the whole of 2017 (where EC data was available) and across all three sites. It was given the
 273 value 8.046. This large-scale version of the TG model gives an estimate of GPP per day.

274 TG3 – Small-scale TG model using MODIS data

275 The small-scale ‘m’ parameter was applied to the large-scale TG model to give an hourly
 276 estimate of GPP using MODIS data.

277 *2.8. Statistical analysis*

278 An Exploratory Factor Analysis (EFA) was used to simplify the large range of variables
 279 measured which could affect GPP on a small scale. EFA is a variable reduction technique
 280 designed to draw out the underlying factors affecting the measured variables. In this case the
 281 EFA was used because we expected that the variables measured were related to each other by
 282 means of underlying constructs, for example, the presence of certain vegetation species was
 283 likely to be correlated due to underlying features of their microhabitats.

284 The variables considered included those explained in Section 2.4 (selected vegetation species,
 285 PAR, surface temperature, soil temperature at 5 cm and 15 cm, soil moisture, and microforms),
 286 and also the NDVI, which is a measure of vegetation greenness and health, and the Normalised
 287 Difference Water Index (NDWI, using NIR and Short-Wave Infrared (SWIR)) which has been
 288 shown to have a relationship with moisture conditions in peatland vegetation (Lees *et al.*,
 289 2019). Repeated measures were accounted for by including the time of year as a variable; in
 290 order to create a linear relationship, daylight period was used as a measure of season. These
 291 variables are referred to in the results by short names given in Table II.

292 **Table II** – Variables used in the EFA, and what they refer to.

Short name	Description
Feather_moss	The proportion of <i>P schreberi</i> in the collar (%)

Reindeer_lichen	The proportion of <i>C portentosa</i> in the collar (%)
S_cap	The proportion of <i>S capillifolium</i> in the collar (%)
Deer_grass	The proportion of <i>T germanicum</i> in the collar (%)
Cotton_grass	The proportion of <i>E angustifolium</i> in the collar (%)
Heather	The proportion of <i>C vulgaris</i> in the collar (%)
NDWI	The calculated NDWI of the collar from the hand-held spectrometer
NDVI	The calculated NDVI of the collar from the hand-held spectrometer
PAR	The average PAR across the clear chamber flux measurement period.
Surface_temp	The temperature amongst the vegetation at the soil surface (°C)
Soil_temp_5cm	The soil temperature at 5 cm depth (°C)
Soil_temp_15cm	The soil temperature at 15 cm depth (°C)
Light_period	Daylight period of the day of measurement in Scotland
microfeature	Whether the collar was on a high area (hummock/ridge) or low area (hollow/ditch)

293

294 The EFA was limited to five factors after initial statistical exploration of different numbers of
 295 factors suggested that this was the best option for all three sites; we found that using five factors
 296 explained the majority of the variance seen in variables at each site (see supplementary
 297 material). The resulting factor scores were correlated with the GPP in order to assess which
 298 factors and variables were most important in determining peatland GPP at small scales, and
 299 whether these could be assessed using remote sensing.

300 All analysis was done in base R (R Core Team, 2017). All results collected specifically for this
 301 study are available online (Lees, Clark, *et al.*, 2019).

302 **3 Results**

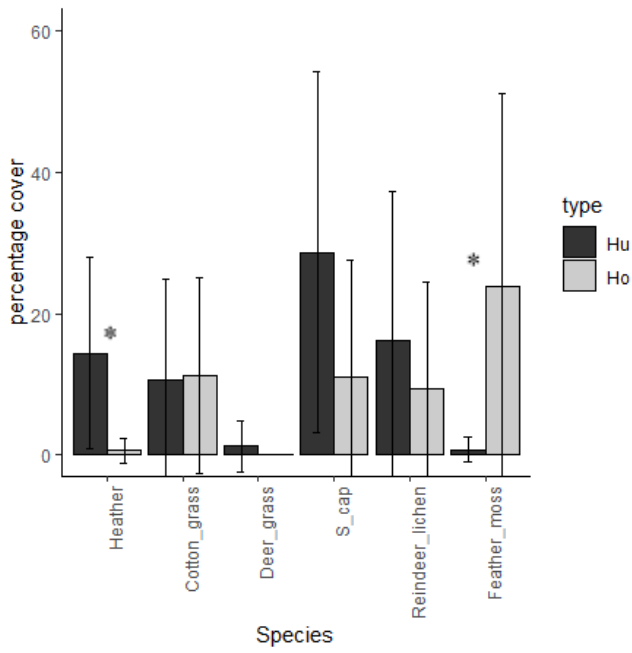
303 *3.1. Factors affecting GPP at small scale*

304 The six vegetation species considered in this analysis show several significant differences
 305 between hummock and hollow percentage coverage (see Figure 2). At the near-natural Cross
 306 Lochs (Figure 2C) site there is significantly more heather (*C vulgaris*) and *S capillifolium* on

307 the hummocks, but significantly more deer grass (*T germanicum*) in the hollows. The Lonielist
308 site (Figure 2A) also has significantly more heather on the hummocks, but significantly more
309 red-stemmed feather moss (*P schreberi*) in the hollows. There were no significant differences
310 between hummock and hollow vegetation at the Talaheel site in 2017 (Figure 2B).

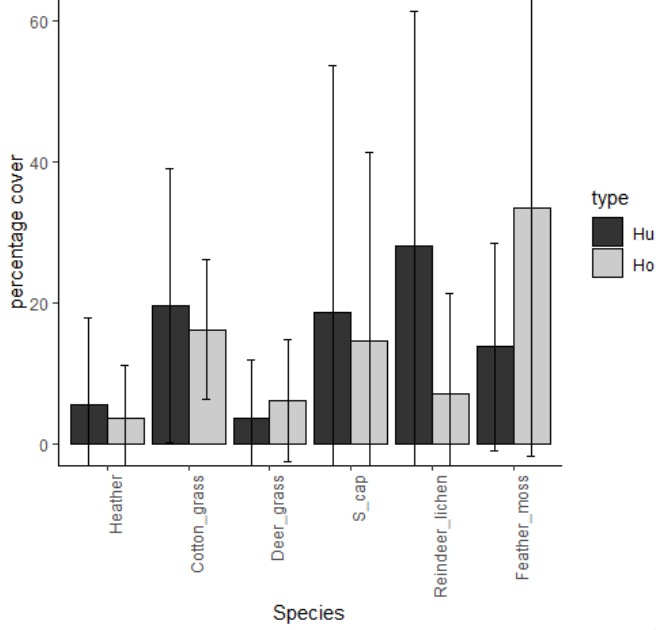
311 There are also differences between the three sites in terms of vegetation cover. Cross Lochs is
312 richer in deer grass than the other two sites, whilst Talaheel has higher cover of common cotton
313 grass (*E angustifolium*). The intact site Cross Lochs also has a greater variety of species, with
314 some present that were not included in our collars at the other two sites such as bog myrtle
315 (*Myrica gale*), bog asphodel (*Narthecium ossifragum*), and sundew (*Drosera rotundifolia*).

A - Lonielist

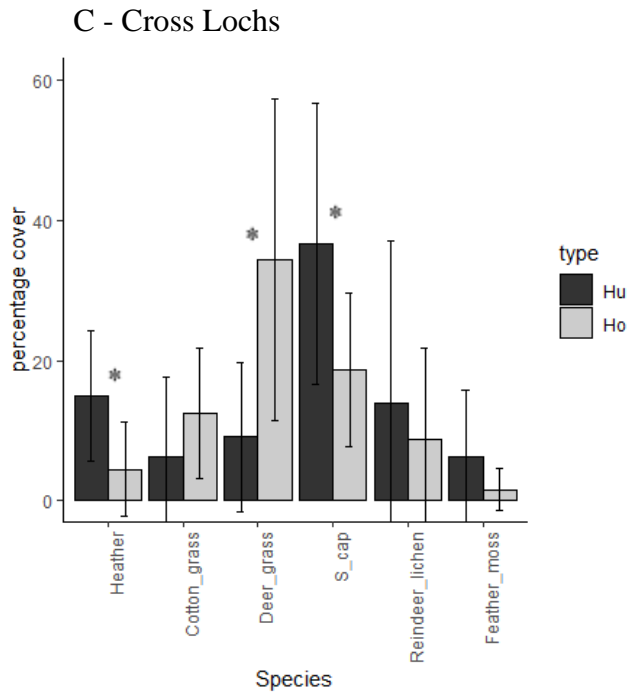


316

B - Talaheel



317



318

319 **Figure 2** –Species differences between hummocks and hollows at the three sites (A: Lonielist, B: Talaheel, C:
 320 Cross Lochs). Stars show significant difference between hummock and hollow (n=8, p<0.05).

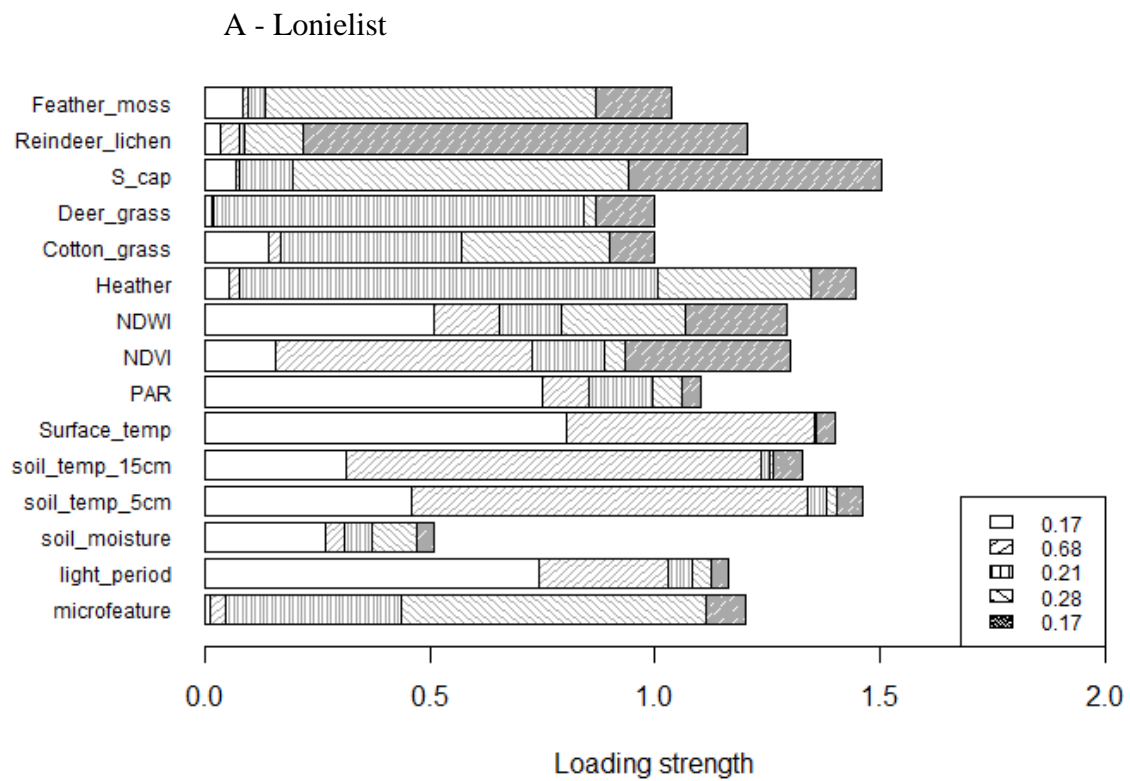
321

322 These selected vegetation species were also used in the EFA, where they are linked to
 323 underlying factors which also affect microtopography (all sites), the NDWI (Talaheel and
 324 Cross Lochs), and soil moisture (Cross Lochs). These factors also correlate with GPP.

325 The EFA results are shown in Figure 3, along with the factor Pearson’s correlations with GPP.
 326 At Lonielist (Figure 3A) the second factor has the highest correlation with GPP (0.68) and is
 327 linked with the NDVI and the three temperature variables. The third and fourth factors also
 328 show some correlation with GPP (0.21, 0.28) and are connected with the microforms variable
 329 and the vegetation species variables.

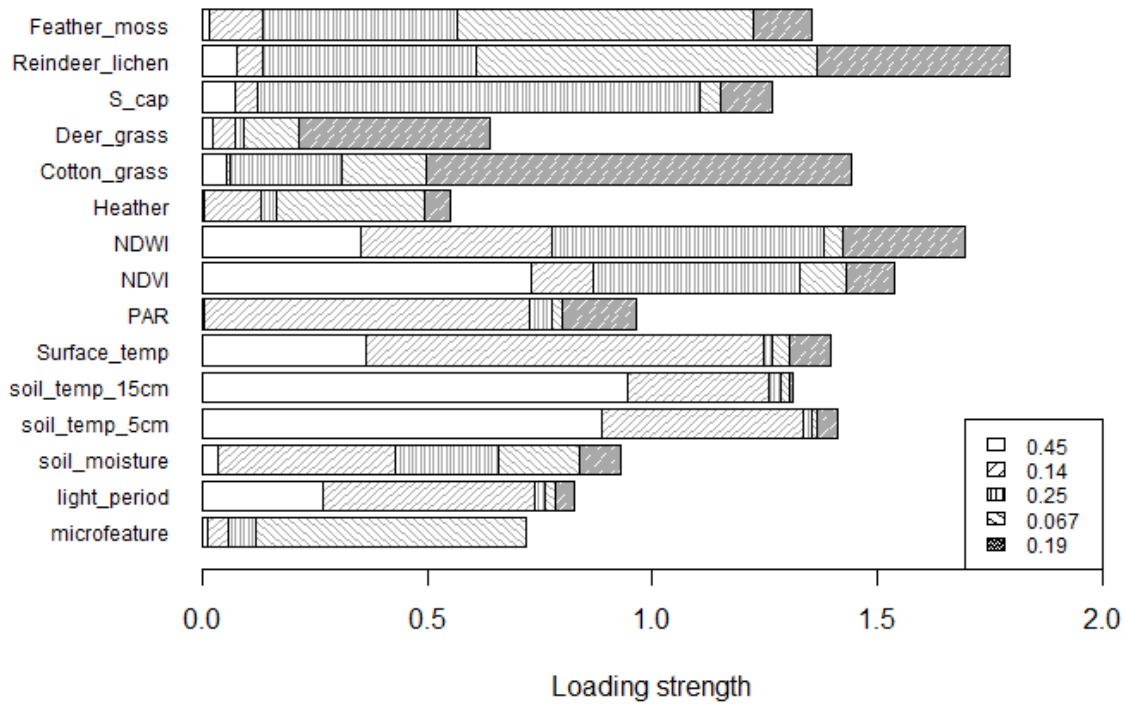
330 At Talaheel (Figure 3B) the first and third factors show correlations with GPP (0.45, 0.25). The
 331 first factor is connected to the NDVI, NDWI, and temperature variables, whilst the third is
 332 linked with the NDWI and NDVI, and percentage cover of *S. capillifolium*, reindeer lichen,
 333 and feather moss.

334 At Cross Lochs the first factor is correlated with GPP (0.49) and links with light period,
 335 temperature, NDWI and PAR. The second factor also correlates with GPP (-0.22) and is
 336 connected to the microform variable, several plant species, soil moisture and the NDWI. The
 337 negative correlation here suggests that the collars classed as hollows have a higher GPP than
 338 those classed as hummocks; this is opposite of the result at Lonielist. The third factor correlates
 339 positively with GPP (0.38) and is connected to the two soil temperature variables, NDWI and
 340 NDVI.



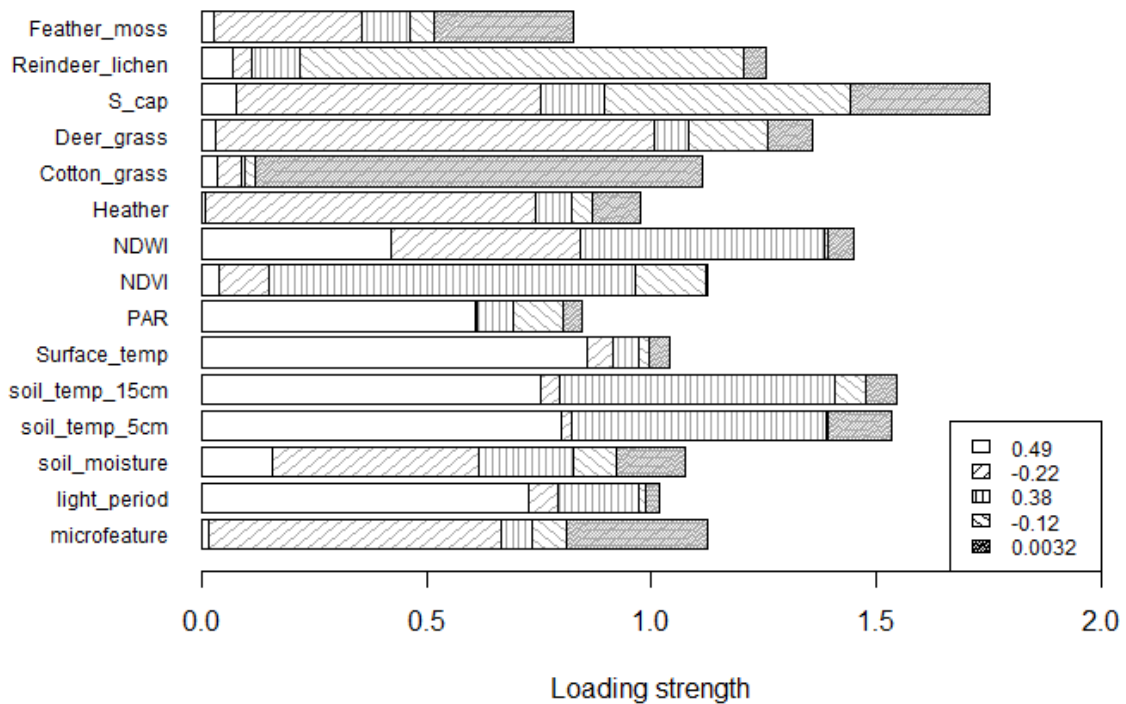
341

B - Talaheel



342

C - Cross Lochs



343

344
345
346
347

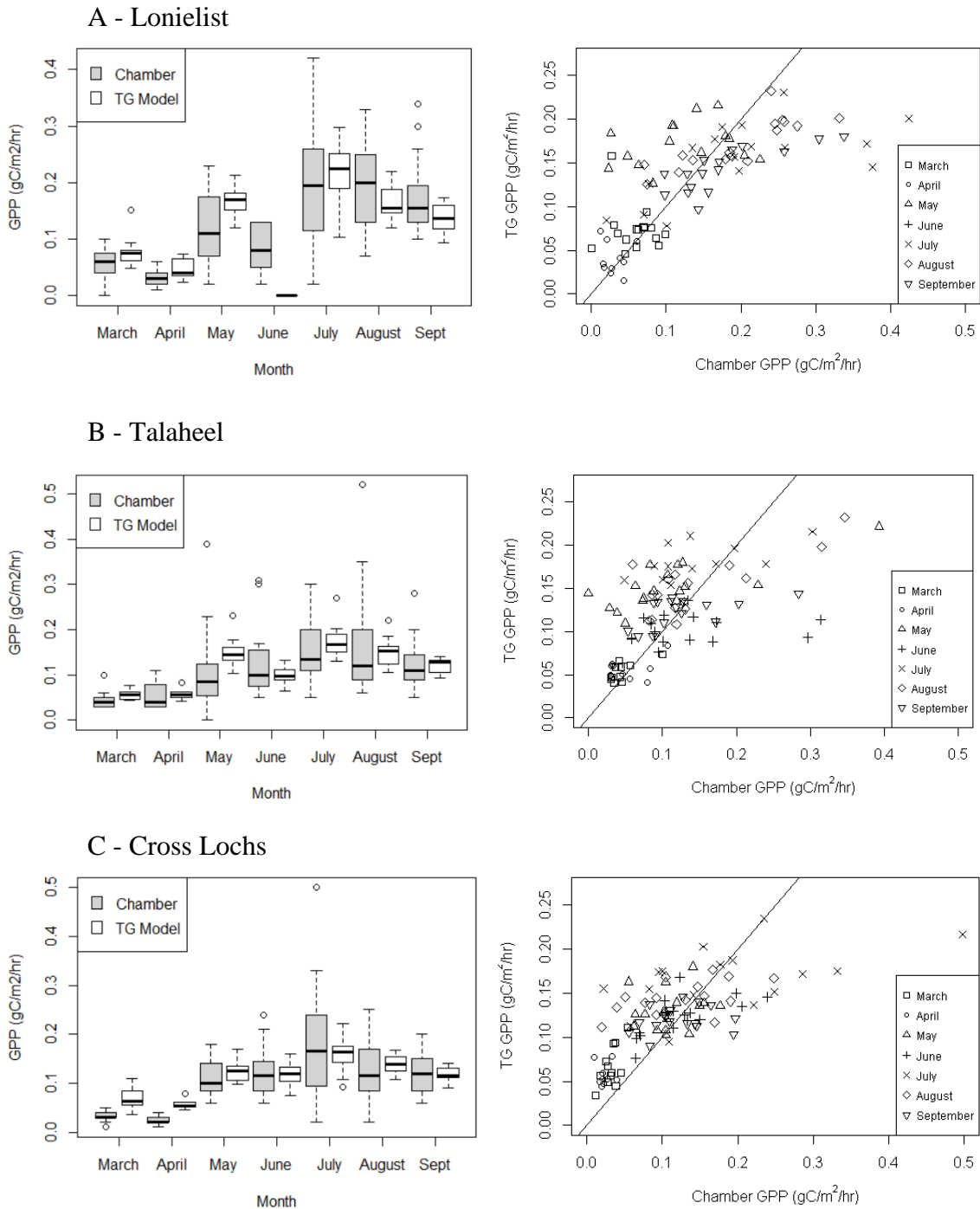
Figure 3 – Lonielist, Talaheel and Cross Lochs factors. Each of the five factors is indicated by a different pattern fill. The variables are given on the y axis, and the factors which underly and are connected with each variable have a loading strength shown by the stacked bar lengths. Legends show correlation of the scores for each factor with GPP values. For example, the first factor at Cross Lochs is shown by the white bars, and has

348 high loading strengths associated with PAR, the three temperature variables, and the light period. It also has a
349 correlation of 0.49 with GPP. See supplementary material for more information.

350

351 *3.2. Comparison of modelled and measured GPP at small scale*

352 Figure 4 shows the TG model using the spectrometer NDVI and the surface temperature
353 applied to each of the sites across the measurement period, with the 'm' parameter calibrated
354 to the chamber data (TG1). The agreement between the model and the chamber data is very
355 good temporally, with the boxplots well within error bars across the year. The chamber fluxes
356 have larger ranges than the TG model results at each site throughout the growing season. The
357 TG model tends to underestimate the highest chamber GPP values, as can be seen from the
358 scatter plots in Figure 4.



359

360 **Figure 4** - Boxplots and scatterplots (by month) comparing the chamber-measured GPP and GPP calculated
 361 from the TG model using hand-held spectrometer data and the surface temperature measurements for each site
 362 (TG1). There is no TG model result in June at Lonielist due to the poor weather causing lack of spectral
 363 measurement. 1:1 lines are plotted on the scatter graphs.

364

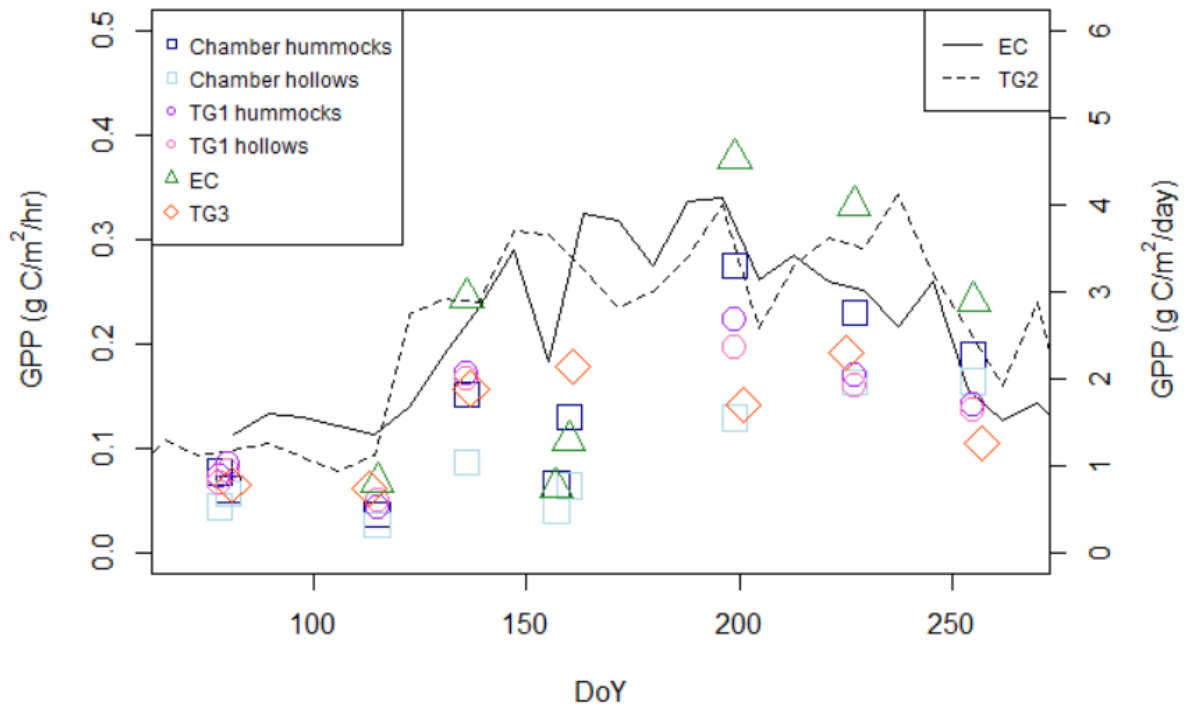
365 *3.3. Comparison of small-scale modelled and measured GPP with EC and satellite data*

366 Figure 5 shows the average GPP across the experiment period from the chamber data and EC
367 data, and modelled from the spectrometer (TG1) and MODIS (TG2 and TG3) data. The
368 Pearson's correlations between the chamber fluxes and the spectrometer TG1 fluxes across all
369 months are 0.57 ($p < 0.01$, $n = 98$) at Talaheel, 0.71 ($p < 0.01$, $n = 89$) at Lonielist, and 0.70 ($p < 0.01$,
370 $n = 101$) at Cross Lochs. TG2 using MODIS data is calibrated on a daily rather than hourly time
371 frame, and the Pearson's correlations between the EC data and the MODIS TG2 model (DoY
372 70 to 265) are 0.76 ($p < 0.01$, $n = 23$) at Lonielist, 0.76 ($p < 0.01$, $n = 24$) at Cross Lochs, and 0.86
373 ($p < 0.01$, $n = 24$) at Talaheel.

374 The chamber GPP is lower than the time-period-matched EC GPP at all three sites (54.9%
375 lower at Lonielist, 72% at Talaheel, 62% at CrossLochs). The TG3 model using MODIS data
376 and the 'm' parameter calibrated from small-scale data matches better with hourly chamber
377 fluxes than EC fluxes.

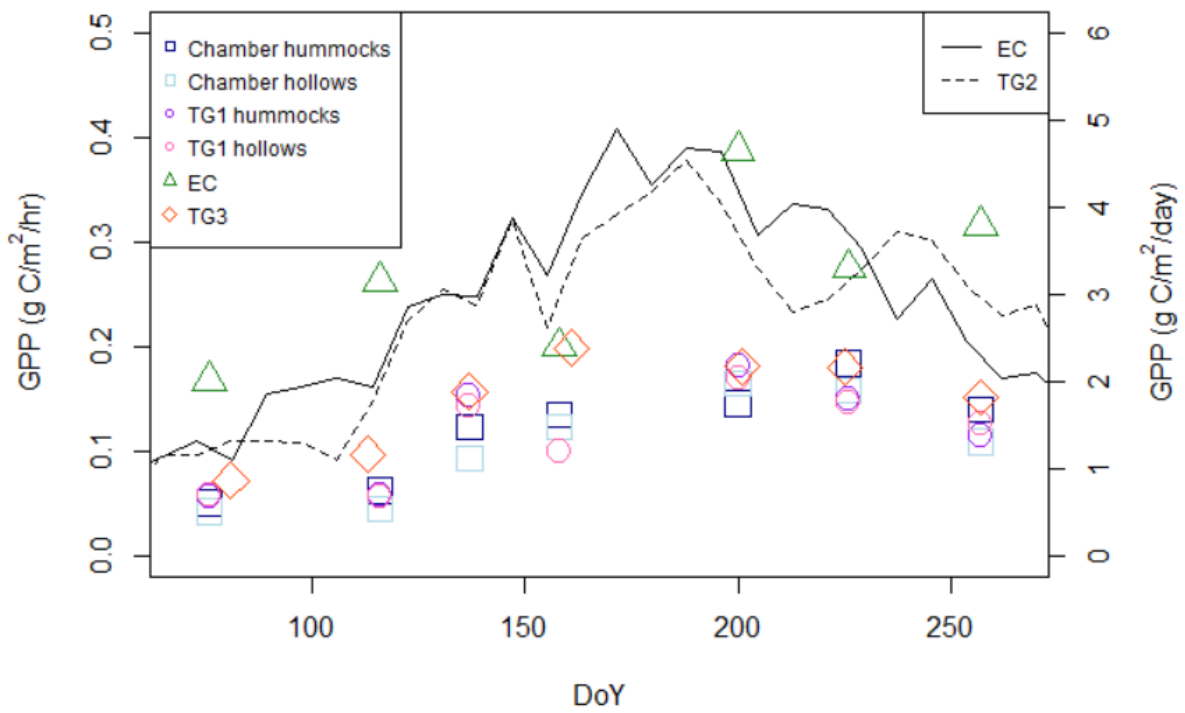
378 The difference between chamber GPP from hummocks and hollows is greatest at Lonielist and
379 shows higher GPP values from hummocks. The difference is less pronounced at Cross Lochs,
380 but shows the opposite effect, with higher GPP from hollows. Talaheel shows less clear
381 differences between the two types of microform. At all three sites the differences in
382 microtopography shown by the spectrometer TG results are less pronounced than those from
383 the chambers. As the differences between GPP from hummocks and hollows are small and
384 inconsistent, area-weighting was not used in upscaling estimates for this study.

A – Lonielist



385

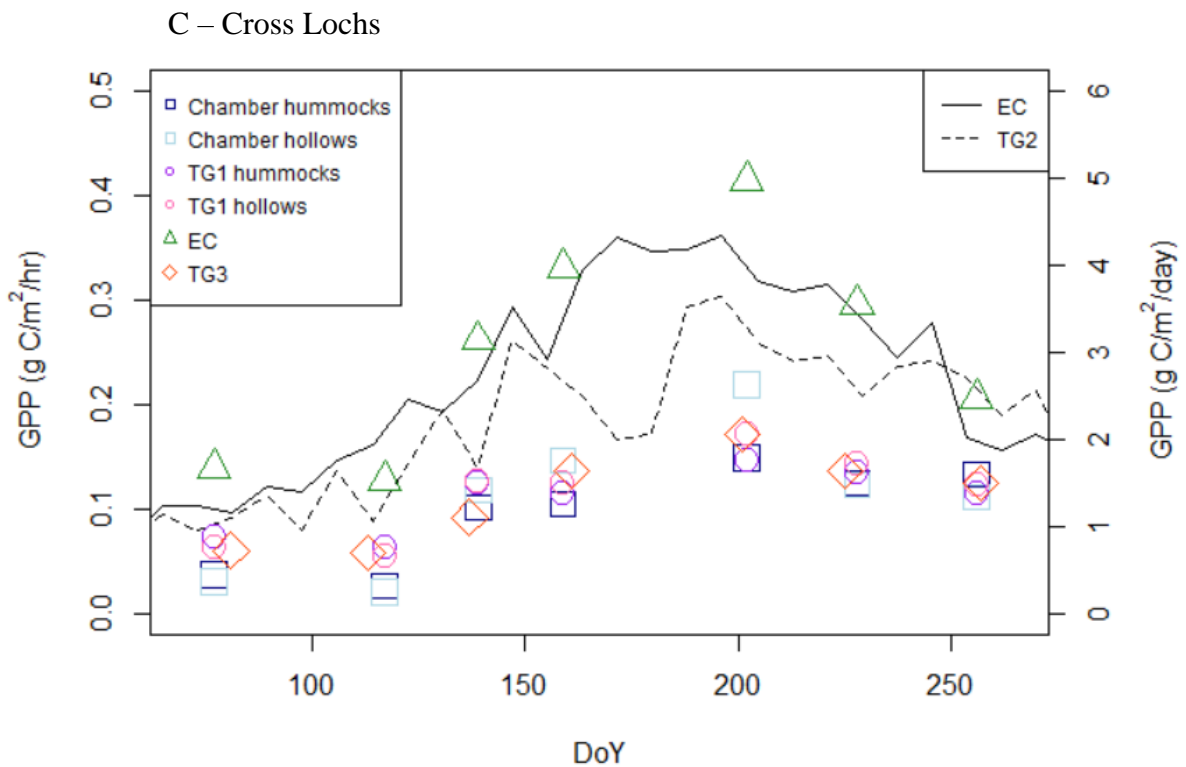
B - Talaheel



386

387

388



389

390 **Figure 5** – The different estimates of GPP for each site across the growing season. The results represented by
 391 coloured symbols and the left-hand axes show the measurements and model results that are calibrated to an
 392 hourly timestep and only calculated during manual field measurement periods. These include the flux chamber
 393 data from hummocks and hollows, the TG1 model results for hummocks and hollows, the EC data averaged
 394 across the half-hourly periods covering the chamber flux measurement period, and the TG3 model. The results
 395 represented by the black lines and the right-hand axes show the measurements and model results that are
 396 calibrated to a daily timestep and are continuous across the growing season of 2017 due to automated measuring
 397 systems. These include the EC data averaged over 8-day periods, and the TG2 model.

398

399

400 **4 Discussion**

401 The EFA correlations with GPP showed that the NDVI and temperature were dominant in the
402 factors affecting GPP at all sites. This endorses the use of the TG model, which makes use of both
403 these variables. All three temperature variables, at surface, 5 cm and 15 cm, were included as
404 variables, but they are strongly related and only one is necessary in the model. The surface
405 temperature provides much more short-term variation compared to soil temperature, and has a
406 relationship with the incoming radiation available for photosynthesis, as shown by the EFA. The
407 variation which surface temperature adds to the model is therefore more than seasonal change, and
408 can provide information on day-to-day changes in GPP due to weather and radiation, and even
409 changes throughout the day.

410 Lonielist GPP results at small scale showed the greatest difference between hummocks and
411 hollows, particularly in July when we had clear skies and high temperatures during the
412 measurement period. This difference may be more evident at Lonielist than the other sites due to
413 the relic furrow and ridge system creating more extreme microtopographical features than would
414 otherwise be found in a blanket bog. Wu et al. (2011) found that there was no difference in
415 simulated GPP using the McGill Wetland Model between hummocks and hollows at the Mer Bleue
416 bog in Canada, consistent with our results from Talaheel, but did find a significant difference in
417 respiration with hummock ecosystem respiration higher than hollows. They showed that shrubs
418 were the dominant influence on hummock carbon cycling, whilst mosses were the dominant factor
419 in hollows. In contrast, Waddington and Roulet (1996) used flux chamber measurements to show
420 that hummocks at their study site in a Swedish peatland had greater CO₂ uptake than hollows
421 during the growing season, similar to our results at Lonielist. It is somewhat surprising that Cross
422 Lochs, the near-natural site, showed a small but opposite difference in fluxes between microforms.

423 Lindsay et al. (1988) found that some areas of the Flow Country were dominated by pool and
424 hollow type landforms due to the wet climate, and it may be the case that our classifications of
425 landforms at Cross Lochs were based on the need to distinguish areas of different heights within
426 close range, and did not always satisfy the descriptions of true hummocks and hollows. In general,
427 the differences in GPP fluxes between microforms did not seem to be large or temporally
428 consistent during our study period. The period during which measurements were taken was
429 generally quite wet, with June, July and August all having higher rainfall totals than the 1981-2010
430 average (Met Office, 2012, 2018). A stronger difference between fluxes from microforms might
431 have been seen under dryer conditions. This is corroborated by previous studies that have found
432 significant differences between carbon fluxes from different microforms linked to soil moisture
433 (Heikkinen *et al.*, 2002; Laine *et al.*, 2006). Despite small differences in GPP among the chamber
434 locations, we did observe significant differences in vegetation between the microtopographical
435 features at Lonielist and Cross Lochs, and also in general between the sites. The significant
436 differences in selected vegetation species are consistent with their preferred microhabitats. Both
437 Lonielist and Cross Lochs show a greater proportion of heather (*C vulgaris*) on the higher areas of
438 ground. Cross Lochs has higher percentages of *S capillifolium*, a *Sphagnum* species well known
439 to be hummock forming (Laine, 2009) on the higher areas, and more deer grass (*T germanicum*)
440 in the hollows, whilst Lonielist has significantly more red-stemmed feather moss (*P Schreberi*) in
441 the furrows. It is worth noting that there is ecological succession in play as well as
442 microtopographical features when we consider these three sites, as shown in Hancock *et al.* (2018).
443 The presence of deer grass (*T germanicum*) seems to be associated more with the near-natural site
444 at Cross Lochs, whilst Talaheel has higher relative proportions of common cotton grass (*E*
445 *angustifolium*) which has been found to colonise disturbed areas of ground (Phillips, 1954).

446 Malhotra *et al.* (2016) similarly found that there was there was a clear relationship between
447 microtopography and species distribution at the Mer Bleue bog in Canada, and that fine spatial
448 structures explained up to 40% of species distribution.

449 The selected vegetation species showed some influence on GPP, although this varied between the
450 sites. The two wetter sites, Cross Lochs and Talaheel, showed greater connections between GPP
451 and measures of moisture, both NDWI and soil moisture measured using the probe. Both Lonielist
452 and Cross Lochs showed some correlations between factors linked with microtopography and
453 GPP, although the relationship was stronger at Lonielist. Malhotra *et al.* (2016) found that water
454 table depth was a significant factor in maintaining distinct vegetation communities on
455 microtopographical features. Their work was done on the Mer Bleue bog in Canada, which can be
456 described as near-natural, and therefore is most similar to our site at Cross Lochs which also had
457 links between microtopography and soil moisture, as shown by the EFA.

458 The underestimation of the model at high GPP values evident in Figure 4 is likely due to the
459 temperature component of the TG model. Although the temperature component functions partly
460 as a proxy for PAR (as shown by the EFA), the relationship between these two factors is not always
461 linear, and this relationship may be even less strong in maritime temperate climates, where warm
462 but cloudy days occur in summer, and cold but clear days in winter. It is worth noting that the
463 presence of vegetation and water bodies can impact the LST (Solangi, Siyal and Siyal, 2019). The
464 values used in the temperature scaling equation may also be affecting the relationship between the
465 model and actual GPP values. These values were estimated visually by plotting EC values against
466 MODIS LST (see Lees, Quaiife, *et al.*, 2019), and may not be completely accurate, particularly at
467 the higher end of the temperature range where we had very little data available.

468 There was a clear difference between the GPP values from the chambers and the EC towers, with
469 the EC data giving higher results at all three sites (Figure 5). There are many possible reasons for
470 this, including errors from the chamber methodology. The collar insertion method, which involved
471 cutting into the peat and root mass around the collar base, could have damaged the vegetation and
472 so reduced chamber fluxes. Heinemeyer et al. (2011) found that collar insertion prior to using a
473 flux chamber could reduce respiration at peatland sites by up to 30-50%, even several months after
474 insertion. The chamber measurements were also subject to a reduction in PAR, which would have
475 resulted in a small reduction measured relative to actual GPP. Background concentrations of CO₂
476 within the chambers were monitored to ensure they were close to atmospheric levels at the start of
477 each measurement, and as the measurements were only five minutes long CO₂ build-up is unlikely
478 to have affected the results. Some of the chamber data showed noise, suggesting that there were
479 minor leaks where the chamber was not perfectly sealed. The data from these measurements was
480 still useable but may show slightly lower results than the actual flux. It is possible that there were
481 some changes in chamber volume throughout the experimental period due to collar settling and
482 vegetation growth which were not accounted for in the measurements and could have led to slight
483 under or overestimation (Morton and Heinemeyer, 2018).

484 Factors affecting the EC fluxes may also be responsible for the differences seen. Cross Lochs,
485 which shows a large difference between EC and chamber GPP results, has an open path sensor
486 compared to the other two sites which have closed paths, and this may have led to inaccuracies in
487 the flux measurements as measurements were only taken during (heavy) rain-free periods and so
488 the gap filling has a degree of bias. (Helbig *et al.*, 2016). The ecosystem respiration results are
489 similar from the chambers and the EC tower (not shown), suggesting that the difference is not
490 caused by the partitioning equations used in EC data processing.

491 Laine *et al.* (2006) compared NEE from EC and chamber measurements at a blanket bog site in
492 Glencar, Ireland, which is climatically and structurally similar to the Forsinard Flows reserve, and
493 found a correlation of 0.82 between EC and interpolated chamber NEE, even when footprint size
494 and direction variation was not accounted for. They did note, however, that agreement decreased
495 towards the extremes of the temperature range, agreeing with the current work where differences
496 were particularly noticeable in the hotter measurement period in July. Griffis, Rouse and
497 Waddington (2000) also compared chamber and EC fluxes, at a subarctic fen in Manitoba. They
498 found that chamber measurements of GPP were 32% lower than EC GPP results, similar to the
499 current work. They also showed that hummocks dominated the CO₂ fluxes, which corresponds
500 with the Lonielist site showing greater agreement between hummock and EC GPP than between
501 hollow and EC GPP. Similarly, Heikkinen *et al.* (2002) found that carbon fluxes from chamber
502 measurements were somewhat lower than those from EC at a subarctic fen in Northern Finland.

503 Application of the TG model with MODIS data and small-scale 'm' parameter (TG3) matched
504 chamber data better than hourly EC data, suggesting that the difference between chamber and EC
505 GPP is not only a result of spatial scale. The TG model is clearly very dependent on calibration to
506 measured data, and therefore the uncertainty of measurements used in the model calibration will
507 form a large part of the uncertainty estimates of the TG model.

508 Generally, the agreement between the TG model and the measured fluxes is shown to be good at
509 small scale (TG1), with correlations of 0.57 to 0.71. The Lonielist and Cross Lochs sites show
510 slightly better agreement than the Talaheel site. Talaheel was also the only site to show almost no
511 connection between microtopography and GPP. This may be due to the recent landscaping of the
512 site to put peat dams in the remaining planting furrows, which has created large flat areas and deep
513 pools, rather than the more natural small hummocks and hollows. It may be the case that the

514 vegetation species have not had time since the work done in 2015/16 to develop their ecological
515 niches. It is also clear that the water levels at Talaheel have been increased by the recent plough
516 furrow blocking, and areas which we would consider hollows are often flooded and so unsuitable
517 for taking flux or spectral measurements. This may also be affecting the agreement with the model,
518 as the Talaheel site might be responding to temperature and seasonal changes differently to sites
519 which have had less recent disturbance.

520 The GPP calculated with the TG model that used data from MODIS (TG2) was strongly correlated
521 with the GPP derived from EC data (correlations of 0.76 to 0.86). This was in agreement with the
522 work done on developing the model in Lees, Quaife, *et al.* (2019). The ‘m’ parameter calibrated
523 for the TG model against EC data in this study, which uses data from 2017, is higher than that
524 calculated in Lees, Quaife, *et al.* (2019) which used 2015/16 data. This may be because the growing
525 season of 2017 was particularly wet; this supports the development of the annual Temperature,
526 Greenness and Wetness (TGWa) model (Lees, Quaife, *et al.*, 2019), which associates high summer
527 wetness with increased annual GPP (this model was not used in this study as it is designed to give
528 a single annual estimate of GPP, and is therefore not applicable on timescales of less than a year).
529 The entirety of the available data were used for optimising the parameterisation in this model, but
530 this does not cause a type 1 error for two reasons: firstly, the ‘m’ parameter does not affect
531 correlation, but only estimate size. Secondly, the error size is only considered in relation to the
532 difference between chamber and EC calibration, and therefore we are not testing the accuracy of
533 the model, but whether the calibration method affects the results.

534 Several previous studies suggest that vegetation indices using finer resolution remote sensing data
535 match EC measurements of GPP better than coarser resolution data across a variety of ecosystems
536 (Fu *et al.*, 2014; Knox *et al.*, 2017; Gonzalez del Castillo *et al.*, 2018). Becker *et al.* (2008) found

537 that hummocks in an oligotrophic pine fen had higher GPP than lawns, and that the percentage
538 cover of hummocks was overestimated when lower resolution imagery was used, resulting in an
539 overestimate of CO₂ uptake. Gatis *et al.* (2017), however, showed that chamber measurements of
540 GPP had strong correlations with vegetation indices calculated from both small-scale camera data
541 and large-scale MODIS data in an upland peatland environment. Similarly, we have found that
542 both small-scale spectrometer data and large-scale MODIS data can be used to give good estimates
543 of GPP in peatland landscapes, but the results are dependent on the calibration. The results of the
544 large-scale TG model using MODIS data gave an average estimate of GPP for the site based on
545 NDVI and LST, and which is not dependent on microfeature classifications. Finer resolution
546 satellites such as Sentinel-2 were not used in this study due to their lack of temperature data
547 meaning that they could not be used to calculate the TG model, but this may become possible in
548 future. Future work should also consider aerial remote sensing as an intermediate scale between
549 field spectrometry and satellite data; data from sensors mounted on both aeroplanes (Carless *et al.*,
550 2019; Räsänen *et al.*, 2019) and Unmanned Aerial Vehicles (UAVs) (Beyer *et al.*, 2019;
551 Scholefield *et al.*, 2019) have begun to be used to assess peatland condition and vegetation
552 communities, and have the potential to be included in methods to estimate carbon fluxes.

553 **5 Conclusions**

554 In this study we have used a Temperature and Greenness (TG) model to estimate GPP from
555 remotely sensed data at small-scale and large-scale, and compared this to chamber and EC
556 measures of GPP.

557 The TG model successfully incorporates the factors which have the greatest relationship with GPP
558 at our study sites as shown by the exploratory factor analysis, and so produces an estimate of GPP

559 that correlates with measured GPP at both small and large scales. Our results suggest that the
560 differences in GPP caused by peatland small-scale heterogeneity are temporally and spatially
561 inconsistent at our study sites, and that the TG model provides an average estimate. Future
562 iterations of the TG model should consider investigating the link between PAR and temperature
563 in more detail, and its effects on the model output, as it is hypothesised that this aspect of the model
564 may cause the underestimation of higher GPP values.

565 The EC results for GPP are larger than those from the chambers, possibly due to several reasons
566 including variation within the tower footprint, and the challenges of collar insertion and chamber
567 methodology. The TG model, however, shows good agreement with the chamber data at small-
568 scale and the EC data at large scale, suggesting that the model design is robust at all scales,
569 although dependent on the calibration data used. The authors can therefore recommend the use of
570 the TG model as a powerful tool for estimating peatland GPP across large areas, but reliable local
571 ground measurements should be used for calibration in order to give accurate values.

572

573 *Conflicts of Interest*

574 The authors declare no conflict of interest.

575 *Acknowledgments*

576 Thanks are due to the RSPB for their work on this project, and for site access and access to
577 facilities. Thanks also to the Environmental Research Institute (ERI) for their role in restoration
578 monitoring at the Forsinard Flows RSPB reserve. Thanks to Graham Hambley, Matthew Saunders,
579 Roxane Andersen and Neil Cowie for site set up and work coordination, and Rebecca McKenzie
580 and Peter Gilbert for site maintenance. Thanks to Kevin White and Suvarna Punalekar for
581 spectroradiometer training. Thanks to Alison Wilkinson for making 48 collars for the fieldwork.

582 We are very grateful for the help of our field assistants Ainoa Pravia, Jose van Paassen, Paul
583 Gaffney, Wouter Konings, Elias Costa, Zsofi Csillag, Valeria Mazzola, David and Parissa
584 Lumsden, and Joe Croft.

585 *Funding*

586 Kirsten Lees was part funded by a studentship from The James Hutton Institute, and part funded
 587 by the Natural Environment Research Council (NERC) SCENARIO DTP (Grant number:
 588 NE/L002566/1). Tristan Quaife was funded by the NERC National Centre for Earth Observation
 589 (NCEO). Myroslava Khomik and Rebekka Artz were funded by The Scottish Government
 590 Strategic Research Programme 2016-2021. Jonathan Ritson was funded by the Engineering and
 591 Physical Sciences Research Council Twenty-65 project [Grant number EP/ N010124/1]. Much of
 592 the restoration work reported in this study was funded by EU LIFE, Peatland Action, HLF, and
 593 the RSPB

594 *References*

595 Arroyo-Mora, J. *et al.* (2018) ‘Airborne Hyperspectral Evaluation of Maximum Gross
 596 Photosynthesis, Gravimetric Water Content, and CO₂ Uptake Efficiency of the Mer Bleue
 597 Ombrotrophic Peatland’, *Remote Sensing*. Multidisciplinary Digital Publishing Institute, 10(4), p.
 598 565. doi: 10.3390/rs10040565.

599 Becker, T. *et al.* (2008) ‘Do we miss the hot spots? – The use of very high resolution aerial
 600 photographs to quantify carbon fluxes in peatlands’, *Biogeosciences*. European Geosciences
 601 Union, 5(5), pp. 1387–1393. doi: 10.5194/bg-5-1387-2008.

602 Belyea, L. R. and Clymo, R. S. (2001) ‘Feedback control of the rate of peat formation’,
 603 268(1473), pp. 1315–1321. doi: 10.1098/rspb.2001.1665.

604 Beyer, F. *et al.* (2019) ‘Multisensor data to derive peatland vegetation communities using a
 605 fixed-wing unmanned aerial vehicle’, *International Journal of Remote Sensing*. Taylor and
 606 Francis Ltd., 40(24), pp. 9103–9125. doi: 10.1080/01431161.2019.1580825.

607 Campbell Scientific (2016) ‘INSTRUCTION MANUAL EASYFLUX DL CR3000OP For
 608 CR3000 and Open-Path Eddy-Covariance System Revision: 3/18’. Available at:
 609 www.campbellsci.com. (Accessed: 9 July 2020).

610 Carless, D. *et al.* (2019) ‘Mapping landscape-scale peatland degradation using airborne lidar and
 611 multispectral data’, *Landscape Ecology*. Springer Netherlands, 34(6), pp. 1329–1345. doi:
 612 10.1007/s10980-019-00844-5.

613 Chapman, S. J. *et al.* (2009) ‘Carbon stocks in Scottish peatlands’, *Soil Use and Management*.
 614 Wiley/Blackwell (10.1111), 25(2), pp. 105–112. doi: 10.1111/j.1475-2743.2009.00219.x.

615 Le Clec’h, S. *et al.* (2018) ‘Mapping ecosystem services at the regional scale: the validity of an
 616 upscaling approach’, *International Journal of Geographical Information Science*. Taylor &
 617 Francis, 32(8), pp. 1593–1610. doi: 10.1080/13658816.2018.1445256.

618 Clement, R. J. *et al.* (2009) ‘Improved trace gas flux estimation through IRGA sampling
 619 optimization’, *Agricultural and Forest Meteorology*. Elsevier, 149(3–4), pp. 623–638. doi:
 620 10.1016/J.AGRFORMET.2008.10.008.

621 Didan, K. (2015) ‘MOD13Q1 V006 | LP DAAC :: NASA Land Data Products and Services’.
 622 NASA EOSDIS LP DAAC. doi: 10.5067/MODIS/MOD13Q1.006.

623 Dinsmore, K. J. *et al.* (2009) ‘Spatial and temporal variability in CH₄ and N₂O fluxes from a
 624 Scottish ombrotrophic peatland: Implications for modelling and up-scaling’, *Soil Biology and*
 625 *Biochemistry*, 41(6), pp. 1315–1323. doi: 10.1016/j.soilbio.2009.03.022.

- 626 European Commission (2018) *Regulation on land use, land use change and forestry in 2030*
 627 *climate and energy framework adopted* / *Climate Action*. Available at:
 628 [https://ec.europa.eu/clima/news/regulation-land-use-land-use-change-and-forestry-2030-climate-](https://ec.europa.eu/clima/news/regulation-land-use-land-use-change-and-forestry-2030-climate-and-energy-framework-adopted_en)
 629 [and-energy-framework-adopted_en](https://ec.europa.eu/clima/news/regulation-land-use-land-use-change-and-forestry-2030-climate-and-energy-framework-adopted_en) (Accessed: 9 July 2018).
- 630 Fratini, G. and Mauder, M. (2014) ‘Towards a consistent eddy-covariance processing: an
 631 intercomparison of EddyPro and TK3’, *Atmospheric Measurement Techniques*. Copernicus
 632 GmbH, 7(7), pp. 2273–2281. doi: 10.5194/amt-7-2273-2014.
- 633 Fu, D. *et al.* (2014) ‘Estimating landscape net ecosystem exchange at high spatial–temporal
 634 resolution based on Landsat data, an improved upscaling model framework, and eddy covariance
 635 flux measurements’, *Remote Sensing of Environment*. Elsevier, 141, pp. 90–104. doi:
 636 10.1016/J.RSE.2013.10.029.
- 637 Gatis, N. *et al.* (2017) ‘Evaluating MODIS vegetation products using digital images for
 638 quantifying local peatland CO₂ gas fluxes’, *Remote Sensing in Ecology and Conservation*.
 639 Edited by N. Pettorelli and M. Disney. Wiley-Blackwell, 3(4), pp. 217–231. doi:
 640 10.1002/rse2.45.
- 641 Gonzalez del Castillo, E. *et al.* (2018) ‘Integrating proximal broad-band vegetation indices and
 642 carbon fluxes to model gross primary productivity in a tropical dry forest’, *Environmental*
 643 *Research Letters*. IOP Publishing, 13(6), p. 065017. doi: 10.1088/1748-9326/aac3f0.
- 644 Griffis, T. J., Rouse, W. R. and Waddington, J. M. (2000) ‘Scaling net ecosystem CO₂ exchange
 645 from the community to landscape-level at a subarctic fen’, *Global Change Biology*. John Wiley
 646 & Sons, Ltd, 6(4), pp. 459–473. doi: 10.1046/j.1365-2486.2000.00330.x.
- 647 Hambley, G. (2016) *The effect of forest-to-bog restoration on net ecosystem exchange in The*
 648 *Flow Country peatlands*. University of St Andrews.
- 649 Hambley, G. *et al.* (2019) ‘Net ecosystem exchange from two formerly afforested peatlands
 650 undergoing restoration in the Flow Country of Northern Scotland.’, *Mires and Peat*, 23, pp. 1–
 651 14.
- 652 Hancock, M. H. *et al.* (2018) ‘Vegetation response to restoration management of a blanket bog
 653 damaged by drainage and afforestation’, *Applied Vegetation Science*. Edited by V. Vandvik.
 654 Wiley/Blackwell (10.1111), 21(2), pp. 167–178. doi: 10.1111/avsc.12367.
- 655 Heikkinen, J. E. P. *et al.* (2002) ‘Carbon dioxide and methane dynamics in a sub-Arctic peatland
 656 in northern Finland’, *Polar Research*. Routledge, 21(1), pp. 49–62. doi:
 657 10.3402/polar.v21i1.6473.
- 658 Heinemeyer, A. *et al.* (2011) ‘Soil respiration: implications of the plant-soil continuum and
 659 respiration chamber collar-insertion depth on measurement and modelling of soil CO₂ efflux
 660 rates in three ecosystems’, *European Journal of Soil Science*, 62(1), pp. 82–94. doi:
 661 10.1111/j.1365-2389.2010.01331.x.
- 662 Helbig, M. *et al.* (2016) ‘Addressing a systematic bias in carbon dioxide flux measurements with
 663 the EC150 and the IRGASON open-path gas analyzers’, *Agricultural and Forest Meteorology*.
 664 Elsevier, 228–229, pp. 349–359. doi: 10.1016/J.AGRFORMET.2016.07.018.
- 665 IUCN (2016) *A Secure Peatland Future A vision and strategy for the protection, restoration and*
 666 *sustainable management of UK peatlands*. Available at: <http://www.iucn-uk->

- 667 peatlandprogramme.org/sites/www.iucn-uk-peatlandprogramme.org/files/CONSULTATION
668 DRAFT A Secure Peatland Future_WEB.pdf (Accessed: 9 July 2018).
- 669 JNCC (2011) *Towards an assessment of the state of UK peatlands*. Available at:
670 http://jncc.defra.gov.uk/pdf/jncc445_web.pdf (Accessed: 3 August 2018).
- 671 Kljun, N. *et al.* (2015) ‘A simple two-dimensional parameterisation for Flux Footprint Prediction
672 (FFP)’, *Geosci. Model Dev*, 8, pp. 3695–3713. doi: 10.5194/gmd-8-3695-2015.
- 673 Knox, S. H. *et al.* (2017) ‘Using digital camera and Landsat imagery with eddy covariance data
674 to model gross primary production in restored wetlands’, *Agricultural and Forest Meteorology*.
675 Elsevier, 237–238, pp. 233–245. doi: 10.1016/J.AGRFORMET.2017.02.020.
- 676 Kross, A., Seaquist, J. W. and Roulet, N. T. (2016) ‘Light use efficiency of peatlands: Variability
677 and suitability for modeling ecosystem production’, *Remote Sensing of Environment*. Elsevier,
678 183, pp. 239–249. doi: 10.1016/J.RSE.2016.05.004.
- 679 Laine, A. *et al.* (2006) ‘Estimating net ecosystem exchange in a patterned ecosystem: Example
680 from blanket bog’, *Agricultural and Forest Meteorology*. Elsevier, 138(1–4), pp. 231–243. doi:
681 10.1016/J.AGRFORMET.2006.05.005.
- 682 Laine, J. (2009) *The intricate beauty of Sphagnum mosses : a Finnish guide for identification*.
683 Department of Forest Ecology, University of Helsinki. Available at:
684 <https://portals.iucn.org/library/node/29078> (Accessed: 13 August 2018).
- 685 Lees, K. J. *et al.* (2018) ‘Potential for using remote sensing to estimate carbon fluxes across
686 northern peatlands – A review’, *Science of The Total Environment*. Elsevier, 615, pp. 857–874.
687 doi: 10.1016/J.SCITOTENV.2017.09.103.
- 688 Lees, K.J., Quaife, T., *et al.* (2019) ‘A model of gross primary productivity based on satellite
689 data suggests formerly afforested peatlands undergoing restoration regain full photosynthesis
690 capacity after five to ten years’, *Journal of Environmental Management*. Academic Press, 246,
691 pp. 594–604. doi: 10.1016/J.JENVMAN.2019.03.040.
- 692 Lees, Kirsten J. *et al.* (2019) ‘Changes in carbon flux and spectral reflectance of *Sphagnum*
693 mosses as a result of simulated drought’, *Ecohydrology*. John Wiley & Sons, Ltd. doi:
694 10.1002/eco.2123.
- 695 Lees, K.J., Clark, J. M., *et al.* (2019) ‘Peatland vegetation: field and laboratory measurements of
696 carbon dioxide fluxes and spectral reflectance’. NERC Environmental Information Data Centre.
697 Available at: <https://catalogue.ceh.ac.uk/documents/ab9f47f9-9faf-4403-a57e-25e31f581ed0>.
- 698 Levy, P. E. and Gray, A. (2015) ‘Greenhouse gas balance of a semi-natural peatbog in northern
699 Scotland’, *Environmental Research Letters*. IOP Publishing, 10(9), p. 094019. doi:
700 10.1088/1748-9326/10/9/094019.
- 701 LI-COR Biosciences (2017) ‘Eddy Covariance Processing Software (Version 7.0.6)’. Available
702 at: www.licor.com/EddyPro.
- 703 Lindsay, R. (2010) *Peatbogs and Carbon: A critical synthesis*. Available at:
704 http://ww2.rspb.org.uk/Images/Peatbogs_and_carbon_tcm9-255200.pdf (Accessed: 9 July 2018).
- 705 Lindsay, R. A. *et al.* (1988) *The Flow Country - The peatlands of Caithness and Sutherland*.
706 Available at: <http://www.jncc.gov.uk/page-4281> (Accessed: 19 October 2018).

- 707 Malhotra, A. *et al.* (2016) 'Ecohydrological feedbacks in peatlands: an empirical test of the
708 relationship among vegetation, microtopography and water table', *Ecohydrology*. Wiley-
709 Blackwell, 9(7), pp. 1346–1357. doi: 10.1002/eco.1731.
- 710 Met Office (2012) 'Met Office Integrated Data Archive System (MIDAS) Land and Marine
711 Surface Stations Data (1853-current).' NCAS British Atmospheric Data Centre. Available at:
712 NCAS British Atmospheric Data Centre.
- 713 Met Office (2018) *Almaharra SAWS climate information - Met Office*. Available at:
714 <https://www.metoffice.gov.uk/public/weather/climate/gfkgdgj2j> (Accessed: 9 July 2018).
- 715 Moore, D. J. P. *et al.* (2013) 'Persistent reduced ecosystem respiration after insect disturbance in
716 high elevation forests', *Ecology Letters*. Edited by J. Penuelas. Wiley/Blackwell (10.1111),
717 16(6), pp. 731–737. doi: 10.1111/ele.12097.
- 718 Morton, P. A. and Heinemeyer, A. (2018) 'Vegetation matters: Correcting chamber carbon flux
719 measurements using plant volumes', *Science of The Total Environment*. Elsevier, 639, pp. 769–
720 772. doi: 10.1016/J.SCITOTENV.2018.05.192.
- 721 Peichl, M. *et al.* (2018) 'Peatland vegetation composition and phenology drive the seasonal
722 trajectory of maximum gross primary production', *Scientific Reports*. Nature Publishing Group,
723 8(1), p. 8012. doi: 10.1038/s41598-018-26147-4.
- 724 Phillips, M. E. (1954) 'Eriophorum Angustifolium Roth', *The Journal of Ecology*. British
725 Ecological Society, 42(2), p. 612. doi: 10.2307/2256893.
- 726 R Core Team (2017) 'R: A language and environment for statistical computing.' Vienna,
727 Austria.
- 728 Räsänen, A. *et al.* (2019) 'Comparing ultra-high spatial resolution remote-sensing methods in
729 mapping peatland vegetation', *Journal of Vegetation Science*. Edited by D. Rocchini. Wiley-
730 Blackwell, 30(5), pp. 1016–1026. doi: 10.1111/jvs.12769.
- 731 Santhana Vannan, S. K. *et al.* (2009) 'A Web-Based Subsetting Service for Regional Scale
732 MODIS Land Products', *IEEE Journal of Selected Topics in Applied Earth Observations and*
733 *Remote Sensing*, 2(4), pp. 319–328. doi: 10.1109/JSTARS.2009.2036585.
- 734 Scholefield, P. *et al.* (2019) 'Estimating habitat extent and carbon loss from an eroded northern
735 blanket bog using UAV derived imagery and topography', *Progress in Physical Geography:*
736 *Earth and Environment*. SAGE Publications Ltd, 43(2), pp. 282–298. doi:
737 10.1177/0309133319841300.
- 738 Sims, D. A. *et al.* (2008) 'A new model of gross primary productivity for North American
739 ecosystems based solely on the enhanced vegetation index and land surface temperature from
740 MODIS', *Remote Sensing of Environment*. Elsevier, 112(4), pp. 1633–1646. doi:
741 10.1016/J.RSE.2007.08.004.
- 742 Solangi, G. S., Siyal, A. A. and Siyal, P. (2019) 'Spatiotemporal Dynamics of Land Surface
743 Temperature and Its Impact on the Vegetation', *Civil Engineering Journal*. Ital Publication, 5(8),
744 pp. 1753–1763. doi: 10.28991/cej-2019-03091368.
- 745 Waddington, J. M. and Roulet, N. T. (1996) 'Atmosphere-wetland carbon exchanges: Scale
746 dependency of CO₂ and CH₄ exchange on the developmental topography of a peatland', *Global*

- 747 *Biogeochemical Cycles*. John Wiley & Sons, Ltd, 10(2), pp. 233–245. doi: 10.1029/95GB03871.
- 748 Wan, Z., Hook, S. and Hulley, G. (2015) ‘MOD11A2 MODIS/Terra Land Surface
749 Temperature/Emissivity 8-Day L3 Global 1km SIN Grid V006’. NASA EOSDIS LP DAAC.
750 doi: 10.5067/MODIS/MOD11A2.006.
- 751 Wang, G. *et al.* (2012) ‘A three-dimensional gap filling method for large geophysical datasets:
752 Application to global satellite soil moisture observations’, *Environmental Modelling & Software*.
753 Elsevier, 30, pp. 139–142. doi: 10.1016/J.ENVSOF.2011.10.015.
- 754 Wu, J. *et al.* (2011) ‘Dealing with microtopography of an ombrotrophic bog for simulating
755 ecosystem-level CO₂ exchanges’, *Ecological Modelling*. Elsevier, 222(4), pp. 1038–1047. doi:
756 10.1016/J.ECOLMODEL.2010.07.015.
- 757 Wutzler, T. *et al.* (2018) ‘Basic and extensible post-processing of eddy covariance flux data with
758 REddyProc’, *Biogeosciences*, 15(16), pp. 5015–5030. doi: 10.5194/bg-15-5015-2018.
- 759 Zhang, N. *et al.* (2007) ‘Scaling up ecosystem productivity from patch to landscape: a case study
760 of Changbai Mountain Nature Reserve, China’, *Landscape Ecology*. Springer Netherlands,
761 22(2), pp. 303–315. doi: 10.1007/s10980-006-9027-9.
- 762